

# Lifetime of the hypertriton

Daniel Gazda<sup>1,\*</sup>, Axel Pérez-Obiol<sup>2</sup>, Avraham Gal<sup>3</sup>, and Eliahu Friedman<sup>3</sup>

<sup>1</sup>Nuclear Physics Institute, 25068 Řež, Czech Republic

<sup>2</sup>Barcelona Supercomputing Center, 08034 Barcelona, Spain

<sup>3</sup>Racah Institute of Physics, The Hebrew University, Jerusalem 9190401, Israel

**Abstract.** Conflicting values of the hypertriton lifetime  $\tau({}^3_{\Lambda}\text{H})$  were derived in relativistic heavy ion (RHI) collision experiments over the last decade. A very recent ALICE Collaboration measurement is the only experiment where the reported  $\tau({}^3_{\Lambda}\text{H})$  comes sufficiently close to the free- $\Lambda$  lifetime  $\tau_{\Lambda}$ , as expected naively for a very weakly bound  $\Lambda$  in  ${}^3_{\Lambda}\text{H}$ . We revisited theoretically this  ${}^3_{\Lambda}\text{H}$  lifetime puzzle [1], using  ${}^3_{\Lambda}\text{H}$  and  ${}^3\text{He}$  wave functions computed within the ab initio no-core shell model employing interactions derived from chiral effective field theory to calculate the two-body decay rate  $\Gamma({}^3_{\Lambda}\text{H} \rightarrow {}^3\text{He} + \pi^-)$ . We found significant but opposing contributions arising from  $\Sigma NN$  admixtures in  ${}^3_{\Lambda}\text{H}$  and from  $\pi^- - {}^3\text{He}$  final-state interaction. To derive  $\tau({}^3_{\Lambda}\text{H})$ , we evaluated the inclusive  $\pi^-$  decay rate  $\Gamma_{\pi^-}({}^3_{\Lambda}\text{H})$  by using the measured branching ratio  $\Gamma({}^3_{\Lambda}\text{H} \rightarrow {}^3\text{He} + \pi^-)/\Gamma_{\pi^-}({}^3_{\Lambda}\text{H})$  and added the  $\pi^0$  contributions through the  $\Delta I = \frac{1}{2}$  rule. The resulting  $\tau({}^3_{\Lambda}\text{H})$  varies strongly with the rather poorly known  $\Lambda$  separation energy  $E_{\text{sep}}({}^3_{\Lambda}\text{H})$  and it is thus possible to associate each one of the distinct RHI  $\tau({}^3_{\Lambda}\text{H})$  measurements with its own underlying value of  $E_{\text{sep}}({}^3_{\Lambda}\text{H})$ .

## 1 Introduction

Hypertriton  ${}^3_{\Lambda}\text{H}$  is the lightest bound hypernucleus with spin-parity  $J^{\pi} = \frac{1}{2}^{+}$  and isospin  $I = 0$ . It can be approximated as a bound state of a  $\Lambda$  hyperon and a deuteron ( ${}^2\text{H}$ ) with tiny  $\Lambda$  separation energy of  $E_{\text{sep}}({}^3_{\Lambda}\text{H}) = 0.148(40)$  MeV [2]. The lifetime of such a loosely bound system is expected to be comparable to the lifetime of the free  $\Lambda$ ,  $\tau_{\Lambda} = 263(2)$  ps [3], which is almost completely (99.7%) governed by its nonleptonic  $\Lambda \rightarrow N + \pi$  weak decay mode. Yet, the world average of measured  ${}^3_{\Lambda}\text{H}$  lifetime,  $\tau({}^3_{\Lambda}\text{H}) = 223^{+12}_{-11}$  ps [4], is by  $\sim 20\%$  shorter than  $\tau_{\Lambda}$ . This so-called ‘hypertriton lifetime puzzle’ has been strengthened recently by the ALICE Collaboration’s  $\tau({}^3_{\Lambda}\text{H})$  value [5] which is consistent with  $\tau_{\Lambda}$  and in tension with previous STAR [6] and HypHI [7] Collaborations measurements. The latest STAR Collaboration’s measurement [8] does not seem to be conclusive since their reported  $\tau({}^3_{\Lambda}\text{H})$  value is consistent within experimental uncertainties with  $\tau_{\Lambda}$  but its central value is 20% shorter. The measured  ${}^3_{\Lambda}\text{H}$  lifetimes from recent RHI experiments together with latest microscopic calculations are summarized in table 1.

---

\*e-mail: gazda@ujf.cas.cz

**Table 1.**  ${}^3_\Lambda\text{H}$  lifetime values (in ps) from recent RHI experiments and theoretical calculations.

Experiment / Theory	$\tau({}^3_\Lambda\text{H})$	Reference
Exp.	$183^{+42}_{-32} \pm 37$	HypHI [7]
Exp.	$142^{+24}_{-21} \pm 29$	STAR [6]
Exp.	$242^{+34}_{-38} \pm 17$	ALICE [9]
Exp.	$221 \pm 15 \pm 19$	STAR [8]
Exp.	$253 \pm 11 \pm 6$	ALICE [5]
Th.	256	Kamada et al. [10]
Th.	$213 \pm 5$	Gal, Garcilazo [11]
Th.	see table 2	Pérez-Obiol et al. [1]
Th.	$\approx \tau_\Lambda$	Hildenbrand, Hammer [12]

## 2 Method

### 2.1 Hypertriton decay

The main channels contributing to the  ${}^3_\Lambda\text{H}$  decay are the  $\pi^-$  and  $\pi^0$  mesonic modes

$$\begin{aligned} {}^3_\Lambda\text{H} &\rightarrow {}^3\text{He}+\pi^-, {}^2\text{H}+p+\pi^-, p+p+n+\pi^-, \\ {}^3_\Lambda\text{H} &\rightarrow {}^3\text{H}+\pi^0, {}^2\text{H}+n+\pi^0, n+n+p+\pi^0 \end{aligned}$$

due to weak-interaction  $\Lambda \rightarrow \pi + N$  and possibly  $\Sigma \rightarrow \pi + N$  transitions, accompanied by the rare non-mesonic modes  ${}^3_\Lambda\text{H} \rightarrow {}^2\text{H}+n, n+n+p$  due to  $\Lambda N \rightarrow NN$ . In this work, we calculate microscopically the two-body  $\pi^-$  decay rate  $\Gamma({}^3_\Lambda\text{H} \rightarrow {}^3\text{He}+\pi^-)$  and evaluate the inclusive  $\pi^-$  decay rate  $\Gamma_{\pi^-}$  by employing the world average experimental branching ratio  $R_3 = \Gamma({}^3_\Lambda\text{H} \rightarrow {}^3\text{He}+\pi^-)/\Gamma_{\pi^-}({}^3_\Lambda\text{H}) = 0.35 \pm 0.04$  [13]. To account for the contribution of the  $\pi^0$  channels, we employ the empirical isospin  $\Delta I = 1/2$  rule, which relates the  $\pi^-$  and  $\pi^0$  rates by  $\Gamma_{\pi^-} = 2\Gamma_{\pi^0}$ . Finally, the non-mesonic  $\Lambda N \rightarrow NN$  and true-absorption  $\pi NN \rightarrow NN$  contributions to the decay rate, are incorporated through a reduction of the  ${}^3_\Lambda\text{H}$  lifetime  $\tau_{\pi}({}^3_\Lambda\text{H}) = 1/\Gamma_{\pi}$  by 1.5% and 0.8%, respectively [14–17]. Here,  $\Gamma_{\pi} = 3/2 \cdot \Gamma({}^3_\Lambda\text{H} \rightarrow {}^3\text{He}+\pi^-)/R_3$  is the inclusive  ${}^3_\Lambda\text{H}$  pionic decay rate obtained using the relations above.

### 2.2 Two-body ${}^3_\Lambda\text{H} \rightarrow {}^3\text{He} + \pi^-$ decay rate

We follow reference [10] and write the two-body  $\pi^-$  decay rate of  ${}^3_\Lambda\text{H}$  as [1]

$$\Gamma^{3\text{He}} = \frac{3}{4\pi} \frac{M_{3\text{He}} q_\pi}{M_{3\text{He}} + \sqrt{m_\pi^2 + q_\pi^2}} \sum_{m^3_\Lambda\text{H}} \sum_{m^3_\text{He}} \left| \langle \Psi_{3\text{He}} \phi_\pi | \hat{O} | \Psi_{3\Lambda\text{H}} \rangle \right|^2, \quad (1)$$

where  $M^3_\Lambda\text{H} = 2991 \text{ MeV}$  and  $M^3_\text{He} = 2809 \text{ MeV}$  are the  ${}^3_\Lambda\text{H}$  and  ${}^3\text{He}$  masses, and  $q_\pi = (2M^3_\text{He})^{1/2} [M^3_\Lambda\text{H} - (m_\pi^2 + 2M^3_\text{He}M^3_\Lambda\text{H} - M^2_{3\text{He}})^{1/2}]^{1/2} = 114.4 \text{ MeV}$  is the pion momentum, with  $m_\pi = 138.04 \text{ MeV}$  the pion mass. The summations run over spin projections  $m^3_\text{He}$  and  $m^3_\Lambda\text{H}$  of the initial  ${}^3_\Lambda\text{H}$  and final  ${}^3\text{He}$  wave functions  $\Psi$  discussed in Sect. 2.3. The  $\phi_\pi$  is the  $\pi^-$  wave function discussed in Sect. 2.4. The operator  $\hat{O}$  due to the weak-interaction  $\Lambda, \Sigma \rightarrow N+\pi$  transitions

$$\frac{\hat{O}}{iG_F m_\pi^2} = \sqrt{2} \left( \mathcal{A}_\Lambda + \frac{\mathcal{B}_\Lambda}{2M_{\Lambda N}} \vec{\sigma} \cdot \vec{q} \right) \hat{P}_{t_{12}=0} + \frac{1}{\sqrt{2}} \mathcal{A}_{\Sigma^-} \hat{P}_{t_{12}=1} \quad (2)$$

contains contributions from  $\Lambda \rightarrow \pi^- + p$ , together with  $\Sigma^- \rightarrow n + \pi^-$  and  $\Sigma^0 \rightarrow p + \pi^-$  due to  $\Sigma NN$  admixtures in the  ${}^3_\Lambda\text{H}$  wave function. The  $\vec{\sigma}$  and  $\vec{\tau}$  are the spin and isospin Pauli matrices,  $G_F m_\pi^2 = 2.21 \times 10^{-7}$ ,  $\vec{q}$  is the pion on-shell momentum, and  $\overline{M}_{\Lambda N} = 1027.3$  MeV is the average  $\Lambda - N$  mass. The parity-violating (PV)  $\mathcal{A}_\Lambda = 1.024$  and parity-conserving (PC)  $\mathcal{B}_\Lambda = -9.431$  amplitudes were extracted from the free  $\Lambda$  lifetime  $\tau_\Lambda = 263(2)$  ps [3], and the PC/PV decay rates ratio [18]. In equation (2), we neglect the PC  $\Sigma$  amplitudes [19], fix the PV  $\Sigma^- \rightarrow n + \pi^-$  amplitude  $\mathcal{A}_{\Sigma^-} = 1.364$  [19] by  $\tau_{\Sigma^-} = 147.9$  ps, and use the  $\chi\text{EFT}$  Lagrangian to relate the  $\Sigma^0 \rightarrow p + \pi^-$  amplitude by  $\mathcal{A}_{\Sigma^0} = \frac{1}{\sqrt{2}} \mathcal{A}_{\Sigma^-}$ . The projection operators  $\hat{P}_{t_{12}}$  select  ${}^3_\Lambda\text{H}$  and  ${}^3\text{He}$  wave function components with a specific isospin  $t_{12}$  of the  $NN$  subcluster. For more details and origin of the numerical factors in equations (1) and (2) see reference [1].

### 2.3 Nuclear and hypernuclear wave functions

The initial- and final-state  ${}^3_\Lambda\text{H}$  and  ${}^3\text{He}$  wave functions in equation (1) are computed within the ab initio no-core shell model (NCSM) approach [20, 21], where nuclei and hypernuclei are described as systems of  $A$  nonrelativistic particles interacting through realistic nucleon–nucleon ( $NN$ ), 3-nucleon ( $NNN$ ) and hyperon–nucleon ( $YN$ ) interactions. In this work we employed a version of NCSM formulated in translationally-invariant relative Jacobi-coordinate harmonic oscillator (HO) basis which is suitable for dealing with few-body systems [22, 23]. The many-body wave function is cast as an expansion in a complete set of basis states

$$|\Psi_E^{J^\pi T}\rangle = \sum_{N=0}^{N_{\max}} \sum_{\lambda} c_{N\lambda}^{J^\pi T} |N\lambda JT\rangle, \quad (3)$$

where the HO states  $|N\lambda JT\rangle$  are characterized by the HO frequency  $\hbar\omega$  and the expansion is truncated by the maximum number  $N_{\max}$  of HO excitations above the lowest configuration allowed by Pauli principle. In equation (3),  $N$  is the total number of HO excitations of all particles and  $J^\pi T$  are the total angular momentum, parity and isospin. The quantum number  $\lambda$  labels all additional quantum numbers and the sum over  $N$  is restricted by parity to an even or odd sequence. The energy eigenstates are obtained by solving the Schrödinger equation

$$\hat{H} |\Psi_E^{J^\pi T}\rangle = E(J^\pi T) |\Psi_E^{J^\pi T}\rangle \quad (4)$$

with the intrinsic Hamiltonian

$$H = \sum_{i=1}^A \frac{\vec{p}_i^2}{2m_i} + \sum_{1 \leq i < j}^{A-1} V_{NN,ij} + \sum_{1 \leq i < j < k}^{A-1} V_{NNN,ijk} + \sum_{i=1}^{A-1} V_{YN,Ai} + \Delta M - H_{\text{CM}}. \quad (5)$$

Here, the masses  $m_i$  and single-particle momenta  $\vec{p}_i$  for  $i \leq A - 1$  correspond to the nucleons and for  $i = A$  to hyperons. The  $H_{\text{CM}}$  is the free center-of-mass (CM) Hamiltonian and the mass term  $\Delta M = \sum_{i < A} m_i - M_0$  with  $M_0$  the reference mass of a hypernuclear system containing only nucleons and a  $\Lambda$  hyperon is introduced to account for the mass difference of coupled  $\Lambda$ - and  $\Sigma$ -hypernuclear states.

For the nuclear  $V_{NN} + V_{NNN}$  interactions in equation (5) we employ the  $\text{NNLO}_{\text{sim}}$  potentials [24] that are based on chiral effective field theory ( $\chi\text{EFT}$ ) up to next-to-next-to-leading order (NNLO). The  $\text{NNLO}_{\text{sim}}$  is a family of 42 different interactions where each potential is associated with one of seven different regulator cutoffs  $\Lambda_{NN} = 450, 475, \dots, 575, 600$  MeV and six different maximum scattering energies in the laboratory system  $T_{\text{Lab}}^{\text{max}} = 125, 158, \dots, 257, 290$  MeV at which the experimental  $NN$  scattering cross sections data base used to constrain the respective interaction was truncated. For the purpose of

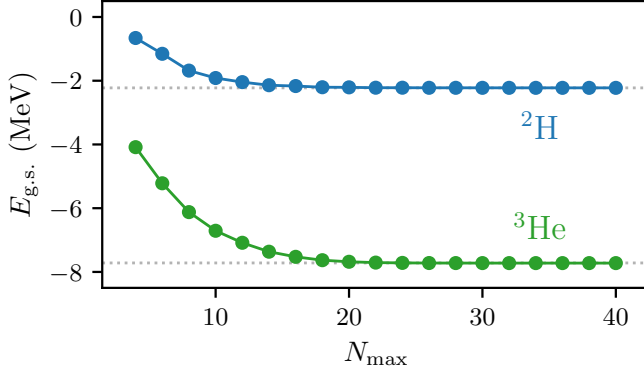


**Figure 1.** Dependence of  ${}^2\text{H}$  and  ${}^3\text{He}$  ground-state energies  $E_{\text{g.s.}}$  on the NCSM model-space truncation  $N_{\text{max}}$  for fixed value of the HO frequency  $\hbar\omega = 14$  MeV, calculated using the  $\text{NNLO}_{\text{sim}}(\Lambda_{\text{NV}} = 500$  MeV,  $T_{\text{Lab}}^{\text{max}} = 290$  MeV) interaction. Experimental values are indicated by the gray dotted lines.

this work precise wave functions of  ${}^3\text{He}$  and the ‘core nucleus’  ${}^2\text{H}$  are required. Since certain low-energy properties of  ${}^2\text{H}$  and  ${}^3\text{He}$  were included in the pool of fit data, their energies are accurately described for all  $\text{NNLO}_{\text{sim}}$  interactions,  $E_{2\text{H},3\text{He}} = -2.224_{(-1)}^{(+0)}, -7.717_{(-21)}^{(+17)}$  MeV [24]. For  $\text{NNLO}_{\text{sim}}$ , the NCSM ground-state (g.s.) energies of  ${}^2\text{H}$  and  ${}^3\text{He}$  exhibit a good convergence with the NCSM model-space truncation  $N_{\text{max}}$  as demonstrated in figure 1 for  $\hbar\omega = 14$  MeV using the  $\text{NNLO}_{\text{sim}}(\Lambda_{\text{NV}} = 500$  MeV,  $T_{\text{Lab}}^{\text{max}} = 290$  MeV)  $NN+NNN$  interaction. The g.s. energies are converged within few keV already at  $N_{\text{max}} \approx 30$  for a wide range of HO frequencies.

For the  $YN$  sector ( $V_{YN}$  in equation (5)) we use the leading order (LO) coupled-channel Bonn–Jülich  $\text{SU}(3)$ -based  $\chi\text{EFT}$  model [25]. The potential consists of pseudoscalar  $\pi$ ,  $K$ ,  $\eta$  meson exchanges and baryon–baryon contact interaction terms. The interaction is regularized by a smooth momentum cutoff  $\Lambda_{YN}$  ranging from 550 to 700 MeV. Unfortunately, calculations of  ${}^3_{\Lambda}\text{H}$  g.s. energy exhibit a slower convergence with the NCSM model-space truncation  $N_{\text{max}}$ . This can be attributed to the very small binding energy of  ${}^3_{\Lambda}\text{H}$  and, consequently, the long tail of the  ${}^3_{\Lambda}\text{H}$  wave function in coordinate space. Nevertheless, well-converged results for the  ${}^3_{\Lambda}\text{H}$  g.s. energy can be obtained for  $N_{\text{max}} \approx 70$  [26]. However, as shown in Sect. 3, it is not possible to achieve full convergence for the transition operator matrix element in equation (1) even in the largest feasible NCSM model spaces and it is necessary to extrapolate the finite-space results into infinite model space. We employ the infrared (IR) extrapolation scheme developed for nuclear NCSM in [27] and generalized recently to hypernuclear NCSM in [28]. In this scheme, the truncation of the HO basis in terms of  $N_{\text{max}}$  and  $\hbar\omega$  is translated into the associated infrared ( $L_{\text{IR}}$ ) and ultraviolet (UV) ( $\Lambda_{\text{UV}}$ ) scales and IR correction formulae can be systematically derived for observables to extrapolate to infinite model space,  $L_{\text{IR}} \rightarrow \infty$ . The LO correction for energies and the expected magnitude of subleading corrections  $\sigma_{\text{IR}}$  [29] are

$$E^{\text{UV}}(L_{\text{IR}}) = E_{\infty}^{\text{UV}} + a_0^{\text{UV}} e^{-2k_{\infty}^{\text{UV}} L_{\text{IR}}}, \quad \sigma_{\text{IR}} \propto \frac{e^{-2k_{\infty}^{\text{UV}} L_{\text{IR}}}}{k_{\infty}^{\text{UV}} L_{\text{IR}}}, \quad (6)$$

where  $(E_{\infty}^{\text{UV}}, a_0^{\text{UV}}, k_{\infty}^{\text{UV}})$  are parameters determined from fit to the NCSM-calculated energies with weights proportional to the inverse of  $\sigma_{\text{IR}}$ . Note that this procedure slightly differs and should improve the one employed in [1]. Additional ultraviolet (UV) corrections to equation (6) can be substantial unless  $\Lambda_{\text{UV}} \gg \Lambda_{\text{MN}}, \Lambda_{\text{YN}}$ . A large-enough  $\Lambda_{\text{UV}}$  scale can be identified by

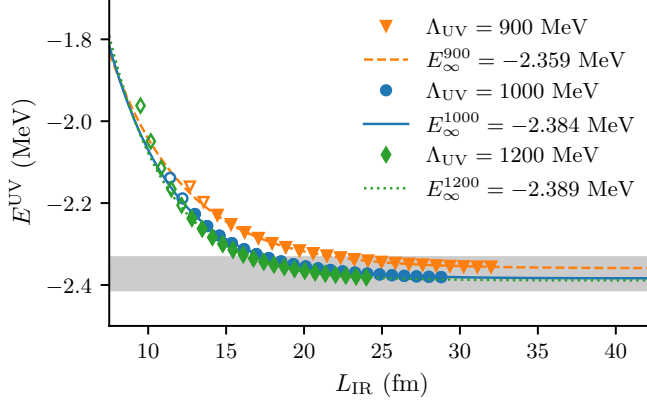


**Figure 2.** The  ${}^3_{\Lambda}\text{H}$  ground-state energies  $E^{\text{UV}}$  as a function of the IR length  $L_{\text{IR}}$  (up to  $N_{\text{max}} = 68$ ) for the NNLO<sub>sim</sub>( $\Lambda_{\text{NV}} = 500$  MeV,  $T_{\text{Lab}}^{\text{max}} = 290$  MeV) and LO YN( $\Lambda_{\text{YN}} = 600$  MeV) interactions, together with their extrapolated values for several fixed values of the UV cutoff,  $\Lambda_{\text{UV}} = 900, 1000, 1200$  MeV. Only the points marked by filled symbols, corresponding to particle-stable  ${}^3_{\Lambda}\text{H}$  configurations, are included in the fits. Experimental value [2] is indicated by the gray shaded area.

performing calculations at a fixed  $\Lambda_{\text{UV}}$ —by choosing appropriate ( $N_{\text{max}}, \hbar\omega$ ) model-space parameters—and monitoring the UV dependence [29]. We find that  $1000 \lesssim \Lambda_{\text{UV}} \lesssim 1200$  MeV is sufficient to achieve UV-convergence and to perform IR extrapolations. This is shown in figure 2 where the  ${}^3_{\Lambda}\text{H}$  g.s. energy  $E_{\Lambda}^{\text{UV}}$  is shown as a function of the IR length  $L_{\text{IR}}$  for several fixed values of the UV scale  $900 \leq \Lambda_{\text{UV}} \leq 1200$  MeV. The NCSM calculations were performed with model space truncation up to  $N_{\text{max}} = 68$  using the NNLO<sub>sim</sub>( $\Lambda_{\text{NV}} = 500$  MeV,  $T_{\text{Lab}}^{\text{max}} = 290$  MeV)  $\text{NN}$  and LO YN( $\Lambda_{\text{YN}} = 600$  MeV) interactions. The extrapolated g.s. energies  $E_{\infty}^{\text{UV}}$  show only a small dependence on the  $\Lambda_{\text{UV}}$  scale of the HO basis once  $\Lambda_{\text{UV}} \gtrsim 1000$  MeV. E.g., for  $\Lambda_{\text{UV}} = 1000(1200)$  MeV, which translates into  $\hbar\omega = 7.299(10.510)$  MeV for  $N_{\text{max}} = 68$ , the finite-space result is  $E_{\Lambda}^{1000(1200)} = -2.3807(-2.3814)$  MeV, while the extrapolated infinite-space result estimated using equation (6) is  $E_{\infty}^{1000(1200)} = -2.384(-2.389)$  MeV.

## 2.4 Pion wave function

The pion wave function in equation (1) was generated from a standard optical potential constrained by data of pionic atoms across the periodic table [30, 31]. In order to extrapolate from the near-threshold region relevant for pionic atoms to  $q_{\pi} = 114.4$  MeV in the  $\pi^{-} - {}^3\text{He}$  CM system, the potential parameters were adjusted using the  $\pi\text{N}$  [32], as well as  $\pi$ -nucleus elastic scattering amplitudes [33, 34].

## 3 Results

In figure 3, we show the 2-body  ${}^3_{\Lambda}\text{H} \pi^{-}$  decay rate  $\Gamma({}^3_{\Lambda}\text{H} \rightarrow {}^3\text{He} + \pi^{-})$  as a function of the HO IR length scale  $L_{\text{IR}}$  (open and filled symbols), together with their extrapolations (solid lines), for several values of the HO basis UV cutoff  $\Lambda_{\text{UV}}$ . Marked by the solid symbols are the points included in the fit which correspond to particle-stable  ${}^3_{\Lambda}\text{H}$  configurations with  $E({}^3_{\Lambda}\text{H}) < E({}^2\text{H})$ . The IR extrapolations were performed by adapting the relations in (6) as  $\Gamma^{\text{UV}}(L_{\text{IR}}) = \Gamma_{\infty}^{\text{UV}} + a_0^{\text{UV}} \exp(-2k_{\infty}^{\text{UV}} L_{\text{IR}})$  with  $(\Gamma_{\infty}^{\text{UV}}, a_0^{\text{UV}}, k_{\infty}^{\text{UV}})$  the fit parameters. This is

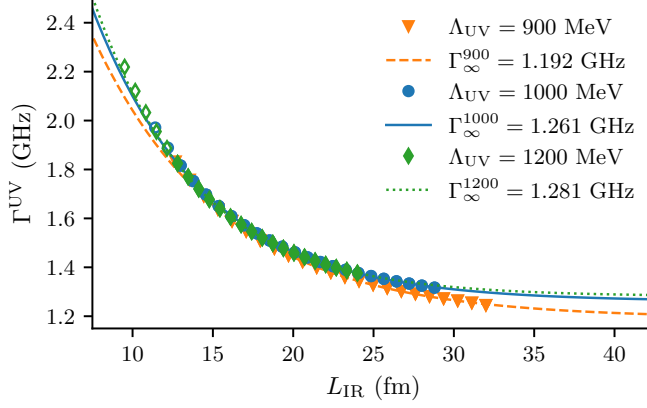


**Figure 3.** The  ${}^3\Lambda\text{H}$  two-body  $\pi^-$  decay rates  $\Gamma^{\text{UV}}$  as a function of the IR length  $L_{\text{IR}}$  (up to  $N_{\text{max}} = 68$ ) for the NNLO<sub>sim</sub>( $\Lambda_{\text{NN}} = 500$  MeV,  $T_{\text{Lab}}^{\text{max}} = 290$  MeV) and LO YN( $\Lambda_{\text{YN}} = 600$  MeV) interactions, together with their extrapolated values for several fixed values of the UV cutoff,  $\Lambda_{\text{UV}} = 900, 1000, 1200$  MeV. The calculated rates include contributions of pion DW as well as  $\Sigma NN$  channels. Marked by filled symbols are the points included in the fits which correspond to particle-stable  ${}^3\Lambda\text{H}$  configurations. The  ${}^3\text{He}$  wave function was held fixed, calculated using  $N_{\text{max}} = 36$  and  $\hbar\omega = 14$  MeV NCSM model space parameters corresponding to a well-converged configuration.

motivated by expanding the rate in powers of  $[E_{\text{sep}}({}^3\Lambda\text{H})]^{1/2}$ , see below. The extrapolated values  $\Gamma_{\infty}^{\text{UV}}$  show only a weak dependence on the UV scale for  $\Lambda_{\text{UV}} \gtrsim 1000$  MeV. The rates in figure 3 are calculated using the NNLO<sub>sim</sub>( $\Lambda_{\text{NN}} = 500$  MeV,  $T_{\text{Lab}}^{\text{max}} = 290$  MeV) and LO YN( $\Lambda_{\text{YN}} = 600$  MeV) interactions and include the effects of  $\pi^-$  DW and  $\Sigma \rightarrow N + \pi$  transitions due to the  $\Sigma NN$  component of the  ${}^3\Lambda\text{H}$  wave function. Replacing the  $\pi^-$  PW by  $\pi^- - {}^3\text{He}$  DW in equation (1) leads to increase of  $\Gamma({}^3\Lambda\text{H} \rightarrow {}^3\text{He} + \pi^-)$  by  $\approx 15\%$ . On the contrary, including the contributions of  $\Sigma \rightarrow N + \pi$  transitions was found to decrease  $\Gamma({}^3\Lambda\text{H} \rightarrow {}^3\text{He} + \pi^-)$  by  $\approx 10\%$ .

The dependence of the extrapolated  $\Lambda$  separation energies  $E_{\text{sep}}^{\text{UV}}$  (figure 2) and 2-body decay rates  $\Gamma_{\infty}^{\text{UV}}$  (figure 3) on the UV scale of the HO basis  $\Lambda_{\text{UV}}$  can be exploited to study the relationship of  $E_{\text{sep}}({}^3\Lambda\text{H})$  and  $\Gamma({}^3\Lambda\text{H} \rightarrow {}^3\text{He} + \pi^-)$ . While the UV convergence for  $\Lambda_{\text{UV}} \lesssim 1000$  MeV was not fully achieved, the calculations still give meaningful, sufficiently IR-converged results. The missing UV corrections to equation (6) depend only on short-range details of the employed interactions truncated by  $\Lambda_{\text{UV}}$ . In table 2, we show the extrapolated  $\Lambda$  separation energies, two-body  $\pi^-$  decay rates, and lifetime values for several HO basis UV scales,  $800 \leq \Lambda_{\text{UV}} \leq 1400$  MeV. The  $\tau({}^3\Lambda\text{H})$  values were deduced from  $\Gamma({}^3\Lambda\text{H} \rightarrow {}^3\text{He} + \pi^-)$  using the procedure detailed in Sect. 2.1, tacitly assuming that the branching ratio  $R_3$  is independent of  $E_{\text{sep}}({}^3\Lambda\text{H})$ . The  $\Lambda$  separation energy rapidly decreases with reducing the UV scale from  $\Lambda_{\text{UV}} = 1200$  MeV to  $\Lambda_{\text{UV}} = 800$  MeV which lowers the two-body  $\pi^-$  rate and enhances  $\tau({}^3\Lambda\text{H})$  due to the vanishing overlap between the wave functions of the loosely bound  ${}^3\Lambda\text{H}$  and  ${}^3\text{He}$ . The small increase in  $E_{\text{sep}}^{\text{UV}}$  for  $\Lambda_{\text{UV}} = 1400$  MeV indicates that higher-order IR corrections to equation (6) become relevant for  $\Lambda_{\text{UV}} \gtrsim 1400$  MeV. The last column of table 2 contains estimated values of  $\Gamma({}^3\Lambda\text{H} \rightarrow {}^3\text{He} + \pi^-)$  and  $\tau({}^3\Lambda\text{H})$  corresponding to the STAR Collaboration's reported value of  $E_{\text{sep}}({}^3\Lambda\text{H}) = 0.41(12)(11)$  MeV [35]. The estimate was obtained by expanding  $\Gamma({}^3\Lambda\text{H} \rightarrow {}^3\text{He} + \pi^-)$  in powers of  $[E_{\text{sep}}({}^3\Lambda\text{H})]^{1/2}$  as  $a[E_{\text{sep}}({}^3\Lambda\text{H})]^{1/2} + bE_{\text{sep}}({}^3\Lambda\text{H})$  and fixing the two expansion parameters ( $a, b$ ) by fitting to the  $E_{\text{sep}}^{\text{UV}}$  and  $\Gamma_{\infty}^{\text{UV}}$  from table 2 for  $800 \leq \Lambda_{\text{UV}} \leq 1200$  MeV. Given the strong dependence of  $\tau({}^3\Lambda\text{H})$  on  $E_{\text{sep}}({}^3\Lambda\text{H})$  and considering

**Table 2.** Extrapolated  ${}^3_\Lambda\text{H}$   $\Lambda$  separation energies, two-body  $\pi^-$  decay rates, and lifetime values for several HO basis UV scales. The  $E_{\text{sep}}^{\text{UV}} = E_{\infty}^{\text{UV}} - E_{2\text{H}}^{\text{UV}}$  is the extrapolated  $\Lambda$  separation energy calculated using the deuteron energy at the corresponding  $\Lambda_{\text{UV}}$  scale. The uncertainty in  $\tau({}^3_\Lambda\text{H})$  comes from the experimental uncertainty in  $R_3$ . The last column shows extrapolations to the STAR Collaboration [35] reported value of  $E_{\text{sep}}({}^3_\Lambda\text{H})$ , see text for details.

$\Lambda_{\text{UV}}$ (MeV)	800	900	1000	1200	1400	–
$E_{\text{sep}}^{\text{UV}}$ (keV)	69	135	160	165	162	410
$\Gamma_{\infty}^{\text{UV}}$ (GHz)	0.943	1.192	1.261	1.281	1.293	1.548
$\tau({}^3_\Lambda\text{H})$ (ps)	$234 \pm 27$	$190 \pm 22$	$180 \pm 21$	$178 \pm 20$	$176 \pm 20$	$147 \pm 17$

the large experimental uncertainty of  $E_{\text{sep}}({}^3_\Lambda\text{H})$ , none of the recent RHI reported  $\tau({}^3_\Lambda\text{H})$  values listed in table 1 can be excluded but, rather can be correlated with its own underlying value of  $E_{\text{sep}}({}^3_\Lambda\text{H})$ .

Aside from the large measurement uncertainties, there are also considerable theoretical uncertainties associated with  $E_{\text{sep}}({}^3_\Lambda\text{H})$  and  $\tau({}^3_\Lambda\text{H})$ . Note that the values listed in table 2 are calculated using a particular hypernuclear Hamiltonian. Recently, we explored the limits of theoretical precision of  $E_{\text{sep}}({}^3_\Lambda\text{H})$  [26, 28] and  $\Gamma({}^3_\Lambda\text{H} \rightarrow {}^3\text{He} + \pi^-)$  due to model uncertainties in  $YN$  and  $NN+NNN$  interactions. For this purpose we employed 4 versions of the Bonn–Jülich LO  $YN$  interaction regularized at  $\Lambda_{YN} = 550, 600, 650, 700$  MeV, together with the whole family of 42 NNLO<sub>sim</sub> nuclear interactions (see Sect. 2.3). Fixing  $\Lambda_{\text{UV}} = 1200$  MeV for IR extrapolations, the combined spread of  $\Lambda$  separation energies for all combinations of  $(\Lambda_{NN}, T_{\text{Lab}}^{\text{max}}, \Lambda_{YN})$  is found to be  $90 \lesssim E_{\text{sep}}({}^3_\Lambda\text{H}) \lesssim 190$  keV, while the spread in calculated two-body  $\pi^-$  rates  $1.0 \lesssim \Gamma({}^3_\Lambda\text{H} \rightarrow {}^3\text{He} + \pi^-) \lesssim 1.4$  GHz, which implies  $160 \lesssim \tau({}^3_\Lambda\text{H}) \lesssim 220$  ps for a fixed value of  $R_3 = 0.35$ . Full details of this study will be presented in our future work.

## 4 Summary

We performed a new microscopic calculation of the hypertriton  $\pi^-$  two-body decay rate  $\Gamma({}^3_\Lambda\text{H} \rightarrow {}^3\text{He} + \pi^-)$  employing  ${}^3_\Lambda\text{H}$  and  ${}^3\text{He}$  three-body wave functions generated by ab initio hypernuclear no-core shell model (Y-NCSM) using realistic  $YN$  and  $NN+NNN$  interactions derived from  $\chi\text{EFT}$ . Using the  $\Delta I = \frac{1}{2}$  rule and the measured branching ratio  $R_3$  to include the remaining  $\pi^0$  and 3- plus 4-body  ${}^3_\Lambda\text{H}$  decay channels, we deduced the  ${}^3_\Lambda\text{H}$  lifetime  $\tau({}^3_\Lambda\text{H})$ . The main findings of this study are: (i) Replacing pionic plane wave (PW) by realistic  $\pi^-$ - ${}^3\text{He}$  distorted wave (DW) enhances  $\Gamma({}^3_\Lambda\text{H} \rightarrow {}^3\text{He} + \pi^-)$  by  $\approx 15\%$ . (ii) The  $\Sigma NN$  admixtures in  ${}^3_\Lambda\text{H}$  reduce the purely  $\Lambda NN$  decay rate by  $\approx 10\%$  due to interference effects, despite their  $\lesssim 0.5\%$  contribution to the norm of the  ${}^3_\Lambda\text{H}$  wave function. (iii) The lifetime  $\tau({}^3_\Lambda\text{H})$  varies strongly with the rather poorly known  $E_{\text{sep}}({}^3_\Lambda\text{H})$ . It is then possible to associate each of the distinct RHI measured  $\tau({}^3_\Lambda\text{H})$  values with its own underlying value of  $E_{\text{sep}}({}^3_\Lambda\text{H})$ . Remarkably, the most recent ALICE Collaboration’s [5]  $E_{\text{sep}}({}^3_\Lambda\text{H}) = 72(63)(36)$  keV central value is almost the same as our lowest  $E_{\text{sep}}^{\Lambda_{\text{UV}}=800} = 69$  keV and our lifetime  $\tau^{\Lambda_{\text{UV}}=800}({}^3_\Lambda\text{H}) = 234 \pm 27$  ps is then consistent with their reported  $\tau({}^3_\Lambda\text{H}) = 253 \pm 11 \pm 6$  ps. Only future experiments expected at MAMI, JLab, J-PARC, and CERN will hopefully pin down  $E_{\text{sep}}({}^3_\Lambda\text{H})$  with a better precision than 50 keV and lead to a resolution of the  ${}^3_\Lambda\text{H}$  lifetime puzzle.

## Acknowledgments

We are grateful to Petr Navrátil for helpful advice on extending the nuclear NCSM codes to hypernuclei; to Johann Haidenbauer and Andreas Nogga for providing us with the input LO

Bonn–Jülich  $YN$  potential; and to Andreas Ekström for providing us the NNLO<sub>sim</sub>  $MN+NNN$  interactions used in the present work. The work of D.G. was supported by the Czech Science Foundation GAČR grants 19-19640S, 22-14497S, and by the European Union’s Horizon 2020 research and innovation program under grant agreement No 824093. Some of the computational resources were supplied by IT4Innovations Czech National Supercomputing Center supported by the Ministry of Education, Youth and Sports of the Czech Republic through the e-INFRA CZ (ID:90140).

## References

- [1] A. Pérez-Obiol, D. Gazda, E. Friedman, A. Gal, Phys. Lett. B **811**, 135916 (2020)
- [2] P. Eckert, P. Achenbach et al., EPJ Web Conf. **271**, 01006 (2022), and Chart of Hypernuclides, <https://hypernuclei.kph.uni-mainz.de>
- [3] P.A. Zyla et al. (Particle Data Group), PTEP **2020**, 083C01 (2020)
- [4] P. Eckert et al., Rev. Mex. Fis. Suppl. **3**, 0308069 (2022)
- [5] ALICE Collaboration (2022), arXiv:2209.07360 [nucl-ex]
- [6] L. Adamczyk et al. (STAR), Phys. Rev. C **97**, 054909 (2018)
- [7] C. Rappold et al., Nucl. Phys. A **913**, 170 (2013)
- [8] M. Abdallah et al. (STAR), Phys. Rev. Lett. **128**, 202301 (2022)
- [9] S. Acharya et al. (ALICE), Phys. Lett. B **797**, 134905 (2019)
- [10] H. Kamada et al., Phys. Rev. C **57**, 1595 (1998)
- [11] A. Gal, H. Garcilazo, Phys. Lett. B **791**, 48 (2019)
- [12] F. Hildenbrand, H.W. Hammer, Phys. Rev. C **102**, 064002 (2020)
- [13] G. Keyes, J. Sacton, J.H. Wickens, M.M. Block, Nucl. Phys. B **67**, 269 (1973)
- [14] M. Rayet, R.H. Dalitz, Nuovo Cim. A **46**, 786 (1966)
- [15] J. Golak et al., Nucl. Phys. A **631**, 740C (1998)
- [16] J. Golak et al., Phys. Rev. C **55**, 2196 (1997), [Erratum: **56**, 2892 (1997)]
- [17] A. Pérez-Obiol, D.R. Entem, A. Nogga, J. Phys. Conf. Ser. **1024**, 012033 (2018)
- [18] M. Ablikim et al. (BESIII), Nature **606**, 64 (2022)
- [19] J.F. Donoghue, E. Golowich, B.R. Holstein, *Dynamics of the standard model*, Vol. 2 (CUP, 2014)
- [20] B.R. Barrett, P. Navrátil, J.P. Vary, Prog. Part. Nucl. Phys. **69**, 131 (2013)
- [21] P. Navrátil, S. Quaglioni, I. Stetcu, B.R. Barrett, J. Phys. G **36**, 083101 (2009)
- [22] D. Gazda, J. Mareš, P. Navrátil, R. Roth, R. Wirth, Few-Body Syst. **55**, 857 (2014)
- [23] R. Wirth, D. Gazda, P. Navrátil, R. Roth, Phys. Rev. C **97**, 064315 (2018)
- [24] B.D. Carlsson et al., Phys. Rev. X **6**, 011019 (2016)
- [25] H. Polinder, J. Haidenbauer, U.G. Meißner, Nucl. Phys. A **779**, 244 (2006)
- [26] T.Y. Htun, D. Gazda, C. Forssén, Y. Yan, Few Body Syst. **62**, 94 (2021)
- [27] K.A. Wendt, C. Forssén, T. Papenbrock, D. Sääf, Phys. Rev. C **91**, 061301(R) (2015)
- [28] D. Gazda, T.Y. Htun, C. Forssén, Phys. Rev. C **106**, 054001 (2022)
- [29] C. Forssén et al., Phys. Rev. C **97**, 034328 (2018)
- [30] E. Friedman, A. Gal, Phys. Lett. B **792**, 340 (2019)
- [31] E. Friedman, A. Gal, Acta Phys. Polon. B **51**, 45 (2020)
- [32] R.A. Arndt, W.J. Briscoe et al., Phys. Rev. C **74**, 045205 (2006)
- [33] E. Friedman et al., Phys. Rev. Lett. **93**, 122302 (2004)
- [34] E. Friedman et al., Phys. Rev. C **72**, 034609 (2005)
- [35] J. Adam et al. (STAR), Nature Phys. **16**, 409 (2020)